Journal of Materials Chemistry

Cite this: *J. Mater. Chem.*, 2012, **22**, 16353

www.rsc.org/materials

PAPER

Different length linkages of graphene modified with metal nanoparticles for oxygen reduction in acidic media

Daekun Kim, Mohammad Shamsuddin Ahmed and Seungwon Jeon*

Received 19th March 2012, Accepted 23rd May 2012
DOI: 10.1039/c2jm31685d

This paper reports the chemical synthesis and experimental characterization of various graphene oxide (GO)-supported platinum (Pt) and palladium (Pd) nanoparticle (NP) catalysts. To investigate the relationship between the linker length and the catalytic activities of the metal-decorated GO catalysts, six samples were prepared with three different linker molecules, $HS(CH_2)_2SH$, $HS(CH_2)_3SH$ and $HS(CH_2)_4SH$ (denoted as GO-*l*-NPs), and two different metal NPs, Pt and Pd. All GO-*l*-NP catalysts were tested in oxygen reduction reaction (ORR) using electrochemical techniques such as cyclic voltammetry (CV) and rotating ring disk electrode (RRDE) hydrodynamic voltammetry to quantitatively obtain the ORR kinetic constants and the reaction mechanisms on a glassy carbon electrode (GCE) in 0.5 M H_2SO_4 solution. All GO-*l*-NPs/GCE electrodes showed significantly improved ORR activity and mechanisms. GO-*l*-NPs were characterized by X-ray photoelectron spectroscopy (XPS), transmission electron microscopy (TEM) and energy-dispersive X-ray spectroscopy (EDS). The results showed that Pt and Pd were successfully attached onto the GO surface. A more positive potential catalytic ORR was observed in the modified GO-*l*-NPs with longer chain linker lengths in both cases.

Introduction

Electrocatalytic oxygen reduction plays a major role in electrochemical energy conversion in fuel cells and metal–air batteries and is equally important for corrosion processes. This reaction has remained the focus of considerable attention because of its complex kinetics and the need for better electrocatalysts for fuel cells.[1–3] The electrocatalytic oxygen reduction reaction (ORR) has attracted extensive interest due to its importance in fuel cells.[4–6] The major problem of oxygen electrocatalysis is the slow kinetics of O_2 reduction.[7]

Graphene, a two-dimensional flat material consisting of monolayer carbon atoms, was discovered by the Geim group in 2004.[8] This carbon material has high mechanical strength, electrical conductivity,[9,10] and surface area,[11,12] and many edge-planes/defects,[13] which make it promising for potential applications in electrochemical fields such as nanoelectronic devices, composite materials,[14] energy-storage, polymer composites, liquid crystal devices and biosensors.[15] Graphene sheets, which have a high specific surface area, unless well separated from each other, tend to form irreversible agglomerates or even restack to form graphite through strong π–π stacking and van der Waals interaction.[16] Preventing aggregation is important because graphene's most useful properties are strongly related to the individual sheets and have been achieved through its covalent modification.[17] Pt is the most commonly used catalyst for ORR in fuel cells, but it is expensive, scarce, and can possibly lead to poisoning from substrate components or by-products.[18] Another problem of existing electrocatalyst technology is the high Pt loading in fuel cell cathodes.[19,20] However, Pd is a good substitute for expensive Pt. These two metal nanoparticle (NP)-modified graphene oxides (GOs) have shown the same results at the same weight percentage.[21] A high metal dispersion[22–24] is an important design factor for ORR catalysts because it conserves expensive metals such as Pt.[22,23] This necessitates the systematic study of the catalytic activity of this material towards ORR for its potential application.[25] The reduced graphene sheet is known to easily form well-aggregated and crumpled structures in solution. GO also has similar structures. Therefore, compared to the studied reduced graphene sheets, the GO has a lower specific surface area and shows degraded mechanical properties and lower conductivity due to the aggregation and crumpling. Recently, the preparation of well-separated graphene sheets has become an important research issue. Some studies have been reported on the use of CNT and linkers for graphene sheet dispersion.[26,27] Since abundant functional groups on the GO surfaces can be used as anchoring sites for metal NPs,[28,29] it is possible to use them as a support to produce graphene–NP hybrids.[30]

This work reports the chemical synthesis and characterization of covalently bonded, GO-based Pt and Pd NP catalysts and their use in 0.5 M H_2SO_4 solution for ORR. The catalytic activities in six GO-*l*-NP samples were investigated using cyclic

Department of Chemistry and Institute of Basic Science, Chonnam National University, Gwangju 500-757, Korea. E-mail: swjeon3380@naver.com

voltammetry (CV) and rotating ring disk electrode (RRDE) hydrodynamic voltammetry in acidic media. The catalysts showed better ORR activity in the longer chain, GO-*l*-NP-modified, glassy carbon electrodes (GCE). Pd-decorated GO had the same catalytic activity with less atomic percentage than Pt-decorated GO. The electrochemical behavior, stability, transferred electron number (n) and formation of H_2O_2 during O_2 reduction were analyzed. The kinetics toward ORR were also analyzed through Koutecky–Levich and Tafel plots. As a result, the linker was used to increase the surface area of crumpled GO, and so metallic NPs at% is increased due to the enhanced possibility of metallic NPs to attach to a wide area. The linker supports GO-*l*-NPs to make stable forms and controls NPs dispersion on the GO surface. Among linkers employed, the longer linker seems to produce high NPs at% and an enhanced catalytic activity towards ORR.

Experimental

Electrochemical setup

Electrochemical techniques, including CV and RRDE voltammetry, were performed using a BAS 100 B/W electrochemical analyzer in a grounded Faraday cage. An EG&GPARC Model 636 RRDE system and a CHI 700C electrochemical workstation bipotentiostat were used for hydrodynamic voltammetry experiments. A conventional three-electrode cell was used consisting of Ag/AgCl (3 M NaCl) as the reference electrode (Bioanalytical Systems), a Pt coil as the auxiliary electrode and a modified rotating GC disk (5 mm in diameter)-pt ring electrode as the working electrode. All potentials were reported with respect to the Ag/AgCl electrode at room temperature. A field emission scanning electron microscope (FE-SEM) image of the modified electrode was obtained on a JSM-7500F field emission scanning electron microanalyzer (JEOL). The high resolution transmission electron microscopy (HRTEM) observations were carried out in a JEM-2200FS microscope at 200 kV. X-ray photoelectron spectroscopy (XPS) was performed using a VGmultilab 2000 spectrometer (ThermoVG Scientific, Southend-on-Sea, Essex, UK) in an ultrahigh vacuum. The XPS data analysis program of Avantage 4.54 version (Thermo electron Corp., England) was used. This system uses an unmonochromatized Mg K (1253.6 eV) source and a spherical section analyzer. Survey scan data were collected using a pass energy of 50 eV. Raman spectra were finally recorded on a LabRam HR800 UV Raman microscope (Horiba Jobin-Yvon, France), KBSI, Gwangju-center. X-ray diffractometry (XRD) was carried out on a X'Pert PRO (PANalytical Corp.).

Graphite powder, 1,2-ethanedithiol, 1,3-propanedithiol, 1,4-butanedithiol, hydrogen hexachloroplatinate(IV) hydrate and potassium tetrachloropalladate(II) were purchased from Aldrich, Korea. $KMnO_4$, H_2SO_4 and H_3PO_4 were purchased from Daejung Co., Korea and were used without any purification.

Preparation of catalysts

Thiolated graphene oxide (tGO). GO was obtained by oxidizing graphite using the improved Hummers method.[31] Four segments of GO and linker materials were separately dispersed together in tetrahydrofuran (THF) into four separate round-bottom flasks and stirred at 50 °C for 20 hours before an hour of ultrasonication. The resulting black materials were separated from the mixture by filtration, washed several times with THF and distilled water (DW), and dried in a vacuum oven at 40 °C for 24 hours. The thiolation was confirmed by XPS.

Metal precursor (Pt and Pd) nanoparticle (NP)-decorated tGO. To verify the support effect, the mixture of GO-*l*-Pt was prepared by adding 30 mg tGO to 30 ml DW for an hour of ultrasonication. Then the metal precursor ($H_2PtCl_6 \cdot xH_2O$ or K_2PdCl_4) dissolved in DW (10 mM) was added and the resulting mixture was stirred for 24 hours at 55 °C. Subsequently, 100 μl of 0.1% $NaBH_4$ (2 ml) solution was injected every 5 minutes. This mixture was filtered and washed three times with DW. Finally, the samples were dried in a vacuum oven at 40 °C for 24 hours to give 23–27 mg of product. In the following discussion, the GO-*l*-Pt samples with $HS(CH_2)_2SH$, $HS(CH_2)_3SH$ and $HS(CH_2)_4SH$ were denoted as samples 1, 2 and 3, and the equivalent GO-*l*-Pd samples as samples 4, 5 and 6, respectively. Fig. 1 shows the total schematic procedures of all synthesized catalysts. In order to compare them with GO-*l*-NPs, GO/Pt and GO/Pd (without linkers) were prepared by a procedure similar to the one above from GO and the metal precursor.

Preparation of working electrodes

An RRDE containing a GC disk and Pt ring sealed in GO-*l*-Pt and GO-*l*-Pd sample holders was polished with 0.05 μm alumina suspension on a polishing cloth (BAS, USA) and cleaned with ultrasonication in DW. After the surface was polished to a mirrored finish, the solution was replaced with 0.5 M H_2SO_4 and hydrogen was evolved at both ring and disk electrodes for 1 min to desorb the chloride ions.[32]

Following cleaning, the dispersed solution was prepared by dispersion of 2.0 mg of each of the six samples and 1.0 ml DW to generate a black solution. For a homogeneous suspension, the solution was sonicated with ultrasonic agitation for 30 minutes. To prepare the GO-*l*-Pt/GCE-modified electrode, 2 × 16 μl of the black solution was cast onto the GCE surface and the solvent evaporated at room temperature. The GO-*l*-Pd samples were prepared by the same procedure. Electrochemical measurements using the GO-*l*-Pt or GO-*l*-Pd modified electrode were conducted in Ar- and O_2-saturated 0.5 M H_2SO_4 solution for the electrocatalytic reduction of O_2.

Results and discussion

SEM characterization

GOs dispersed in solution are characterized by layered well-aggregated and crumpled structures. These properties are changed by the linker. Due to the linker the GO surface is stretched and separated. These scheme images are shown in Fig. 2. This means broadening the surface area. So, many metal NPs have increased the possibility of attaching to the surface. Fig. 2D and E show FE-SEM images of GO and GO-linker. The aggregation and separation of GO and a linker containing GO, respectively, were confirmed by these FE-SEM images.

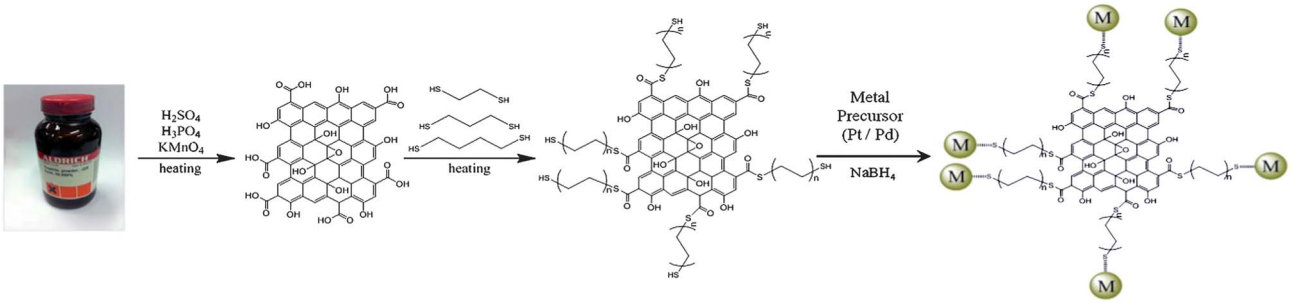

Fig. 1 Schematic procedures for the preparation of the metal catalysts on the tGO (where $n = 2, 3, 4$).

XPS characterization for all six catalysts

The GO, tGO, GO-*l*-Pt and GO-*l*-Pd samples were first characterized by XPS (Fig. 3). The criterion for each peak was based on C 1s 285 eV. Fig. 3A shows a series of XPS survey spectra obtained from GO, tGO and six samples of Pt- and Pd-decorated GO. The XPS data for GO show distinct C and O 1s peaks only and no other elements were detected. tGO presented the same results except for a distinct S 2p peak at 164 eV, indicating that the S-containing linkers were attached successfully. The strong Pt 4f peaks were evident for the GO-*l*-Pt samples along with C 1s and O 1s peaks, indicating the growth of numerous Pt NPs deposited from Pt precursors on the tGO. The Pt^0 at% was estimated as 0.46%, 0.53% and 0.67% for samples 1, 2 and 3, respectively. Nevertheless, strong Pd 3d peaks appeared for the GO-*l*-Pd samples along with the C 1s and O 1s peaks, suggesting that numerous Pd NPs were deposited from Pd precursors on the tGO. The Pd^0 atomic percentage was also estimated as 0.62%, 0.75% and 0.98% for samples 4, 5 and 6, respectively (Table 1).

We believe that the two types of metal NPs were formed by the covalent bonding with S that had already been placed on the surface of GO. Fig. 3B shows the core level peaks of Pt 4f for all Pt-containing samples. Precise cleaving of the Pt 4f peak divided it into two peaks. The binding energy of three samples, 71.70 eV, 71.22 eV and 71.46 eV, respectively, is similar to the previously known Pt^0 binding energy of 71.2 eV.[33] Fig. 3C shows the core level peaks of Pd 3d for all three Pd-containing samples. Distinct Pd^0 peaks appeared at 338.2 eV and 343.2 eV for $3d_{5/2}$ and $3d_{3/2}$, respectively. Based on XPS data, when the metal atomic% was increased a long chain containing a linker can probably be attached to GO and metal NPs perfectly. As a result, the Pt^0 and Pd^0 atomic% were increased significantly. Fig. 4 shows the C 1s XPS peaks of GO and three different tGOs. The spectrum of GO, in Fig. 4A, can be de-convoluted into three different peaks that correspond to carbon atoms by assuming different binding states. On the other hand, a new peak was observed on the C 1s peak of the other three samples. The binding energy of this new peak was identified as corresponding to the CH_2 chain,[34] indicating that the $–CH_2–$ chain-containing thiol linkers had successfully attached to the GO surface with the reduction of the –C–O peak.

HRTEM, SAD pattern and XRD investigation for prepared catalysts

Fig. 5 shows the typical HRTEM images of GO-*l*-NPs. As shown in Fig. 5A, the TEM images of GP-*l*-Pt show that GO was decorated with Pt NPs that were strongly adhered on the outside

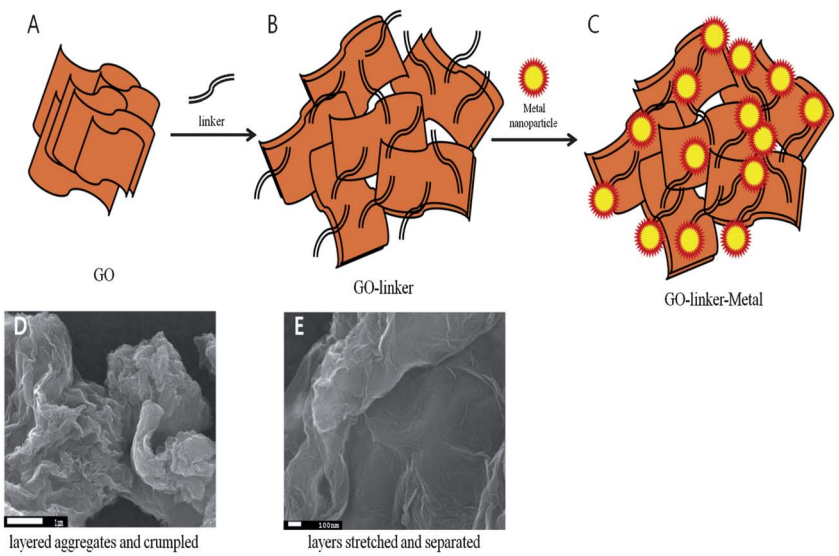

Fig. 2 Scheme for preparing GO (A), GO-linker (B) and GO-*l*-NPs (C), FE-SEM image of aggregates and crumpled GO (D) and more starched and separated GO-linker (E).

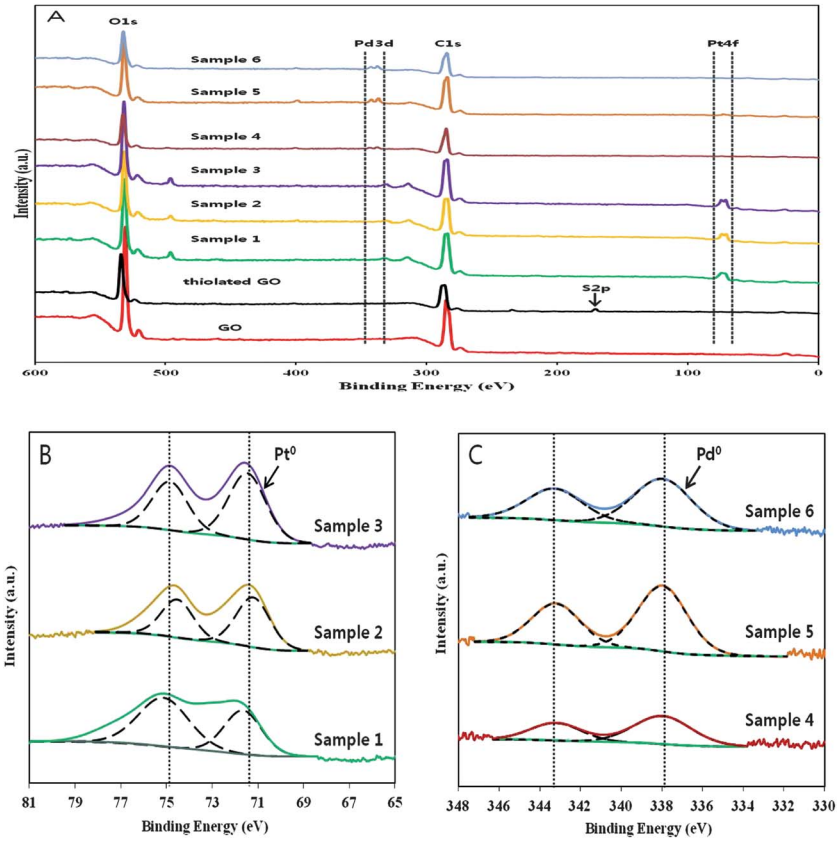

Fig. 3 XPS survey spectra of GO, tGO, GO-*l*-Pt (samples 1–3) and GO-*l*-Pd (samples 4–6) (A), core level XPS spectra of Pt 4f (B) and Pd 3d (C) of the respective samples.

of the GO. The NPs were sized at approximately 3–5 nm. The energy-dispersive X-ray spectroscopy (EDS) analysis shown in the inset of Fig. 5A and B shows that the species supported on the GO was Pt. Nevertheless, the HRTEM images of GO-*l*-Pd show that GO was decorated with Pd NPs on the outside of the GO (Fig. 5B). The NPs were sized at approximately 3–5 nm. The EDS analysis shown in the inset of Fig. 5B shows that the species supported on the GO was Pd. The NPs lattice image can be understood better from Fig. 5C and D.

In addition, detailed descriptions for the existence of the crystalline structure of the Pd and Pt NPs in these samples have been obtained from the HRTEM image and selected area diffraction (SAD) pattern shown in Fig. 5, respectively. Fig. 6 shows the XRD analysis of the corresponding crystalline structures for the Pt and Pd NPs, with peaks at 39.9°, 46.3°, 67.6° and 81.5° for the Pt NPs, and at 40.1°, 46.7°, 68.1° and 82.0° for the Pd NPs, respectively, to the diffraction of the (111), (200), (220) and (311) planes of the face-centered cubic metal crystal with the same space group (*Fm*3*m*).[35,36] Also, a *d*-spacing value shown in Fig. 5 was obtained from XRD data of Fig. 6, and the sample exhibits lattice planes with a 0.22 nm inter-planar distance and a mean particle size of 3 to 10 nm. The distribution of the metal nanocrystallite appeared to be homogeneous. The data identify that cubic crystalline phases of Pt and Pd are present in the samples. According to the results of HRTEM and SAD experiments, measurements are similar to the Joint Committee of Powder Diffraction Standards (JCPDS).[37] Therefore, we conclude that Pt and Pd NPs were attached to GO-linkers.

Raman characterization of GO-*l*-NPs

The Raman spectrum of graphite was already reported, as well as the intense G band at 1564 cm^{-1} and the weak D band at 1344 cm^{-1}. The ratio of the intensities of the D and G bands, I_D/I_G, is frequently used as a measure of the degree of structural defects.[38] The Raman spectrum of GO is shown in Fig. 7A, the G and D bands shift to 1598 cm^{-1} and 1353 cm^{-1}, respectively. The Raman spectra of sample 3 (Fig. 7B) and sample 6 (Fig. 7C)

Table 1 Pt and Pd atomic percentage of six samples

	Pt^0 atomic%		Pd^0 atomic%
Sample 1: GO–S–$(CH_2)_2$–S–Pt	$0.46 \pm 9.2 \times 10^{-4}$	Sample 4: GO–S–$(CH_2)_2$–S–Pd	$0.62 \pm 1.2 \times 10^{-3}$
Sample 2: GO–S–$(CH_2)_3$–S–Pt	$0.53 \pm 1.1 \times 10^{-3}$	Sample 5: GO–S–$(CH_2)_3$–S–Pd	$0.75 \pm 1.5 \times 10^{-3}$
Sample 3: GO–S–$(CH_2)_4$–S–Pt	$0.67 \pm 1.3 \times 10^{-3}$	Sample 6: GO–S–$(CH_2)_4$–S–Pd	$0.98 \pm 1.9 \times 10^{-3}$

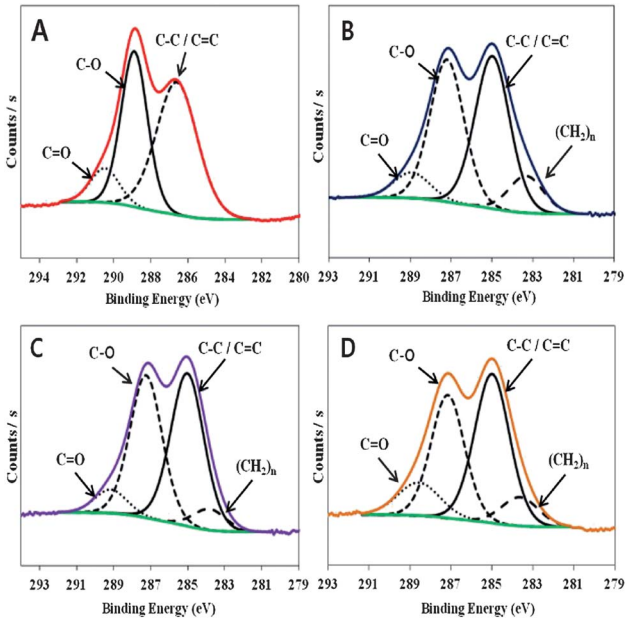

Fig. 4 Core level C 1s XPS spectra of GO (A), three different linkers containing tGO: HS–$(CH_2)_2$–SH (B), HS–$(CH_2)_3$–SH (C) and HS–$(CH_2)_4$–SH (D).

cause the G bands of sample 3 and sample 6 to shift slightly to higher wavenumbers, 1600 cm^{-1} and 1599 cm^{-1}, respectively.

The I_D/I_G ratios of sample 3 and sample 6 decrease from 1.05 (GO) to 0.95 (sample 3) and 0.96 (sample 6), respectively. The result indicates that GO-*l*-NPs are a reduced form when compared with GO, and the conductivity of GO-*l*-NPs may be increased. Also, there are positive shifts from 2698 cm^{-1} for GO as a 2D-band peak to 2708 cm^{-1} for sample 3 and 2723 cm^{-1} for sample 6, respectively.

Electrocatalytic O_2 reduction on six sample/GCEs

Typical CVs were taken in Ar- and O_2-saturated 0.5 M H_2SO_4 solutions, and all had potentials ranging from +0.6 V to −0.2 V at a scan rate of 100 mV s^{-1} for the six catalysts shown in Fig. 8. The three samples of GO-*l*-Pt/GCE electrode were used for the reduction of molecular oxygen in this study *via* CV. The peak potential of the dioxygen reduction wave appeared for the GO-*l*-Pt-coated electrodes (Fig. 8A). There was a negligible peak potential for Ar-saturated CV; a peak potential appeared for each sample in the O_2-saturated CVs for the three GO-*l*-Pt samples. The half-wave potentials ($E_{1/2}$) were 0.17 V, 0.23 V, and 0.29 V for samples (1), (2), (3) with a current of 28.7 μA, 31.2 μA, and 33.6 μA, respectively. For the GO-*l*-Pd-coated electrodes (Fig. 8B), there was no peak potential for Ar-saturated CV. For samples (4), (5) and (6), the $E_{1/2}$ was 0.07 V, 0.18 V and 0.25 V with a current of 31.9 μA, 30.9 μA, and 31.2 μA, respectively in the O_2-saturated acid media. Meanwhile, the $E_{1/2}$ of GO/Pt and GO/Pd was 0.11 V and −0.04 V with a current of 6.3 μA and 18.1 μA, respectively. The catalytic activity of GO/NPs was lower than that of GO-*l*-NPs. The reason that GO-*l*-NPs had an enhanced catalytic activity is ascribed to the strong chemical bonding (GO-*l*-NPs) between GO and metal NPs by linker molecules rather than the weak adsorption (GO/NPs) between

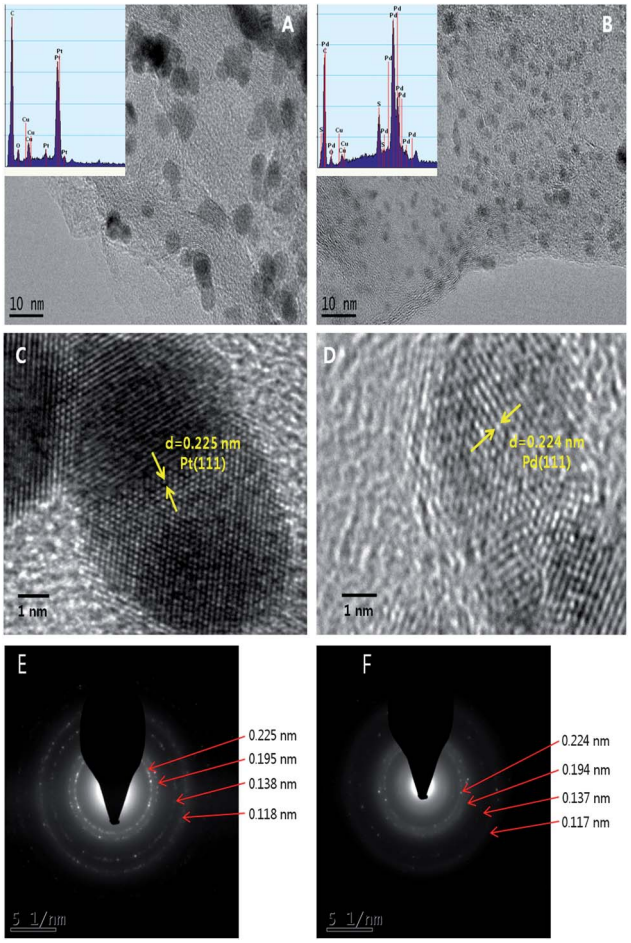

Fig. 5 HRTEM image of GO-*l*-Pt image (A), GO-*l*-Pd image (B), enlarged image of a Pt particle (C) and Pd nanoparticles (D), SAD pattern of the GO-*l*-Pt (E) and GO-*l*-Pd (F) and inset: corresponding EDS spectrum.

GO and metal NPs without linkers. Consequently, GO-*l*-NPs had an enhanced catalytic effect when compared with GO/NPs. Among three GO-*l*-NPs, the longer carbon chain gave well-dispersed GO sheets and high M^0 at% (0.46%, 0.53% and 0.67% for Pt samples 1, 2 and 3, and 0.62%, 0.75% and 0.98% for Pd samples 4, 5 and 6). Therefore, the linker molecule makes stable GO-*l*-NPs and controls the NP distribution on the GO surface. These results of the longer carbon chain seem to produce an enhanced catalytic activity towards ORR. The performance of GO-*l*-NPs for ORR is comparable to the reported catalysts[39,40] without linkers even though metal NPs at% is low in GO-*l*-NPs.

Hydrodynamic voltammetry study

To analyze the experimental results in this study, we used a simplified model[41] of ORR, as shown in Scheme 1. Path 1 shows how O_2 is reduced directly to H_2O through a four-electron transfer. Path 2 is the sequential reaction path where O_2 is first reduced to H_2O_2 through a two-electron transfer followed by a two-electron reduction to H_2O (path 3), or by the release of the formed H_2O_2 into bulk solution (path 4).

The RRDE hydrodynamic voltammetry experiments were useful in confirming the electrocatalytic reduction pathway of

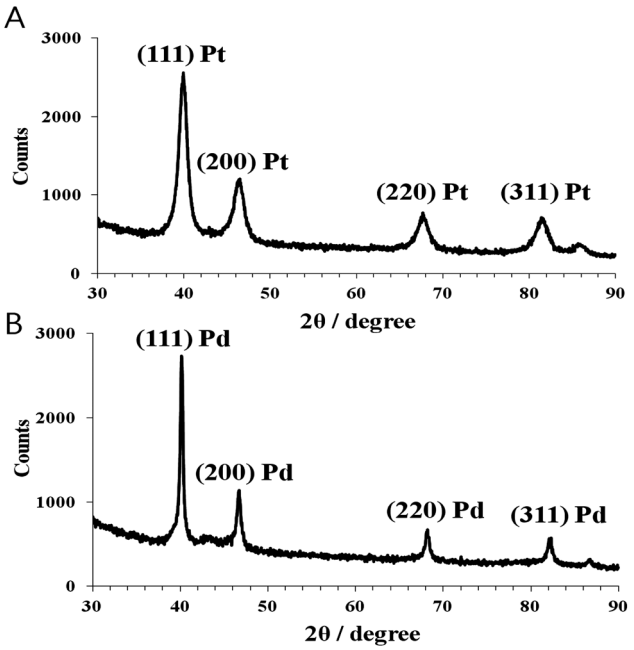

Fig. 6 XRD patterns of Pt (A) and Pd (B) nanoparticles of GO-*l*-NPs samples.

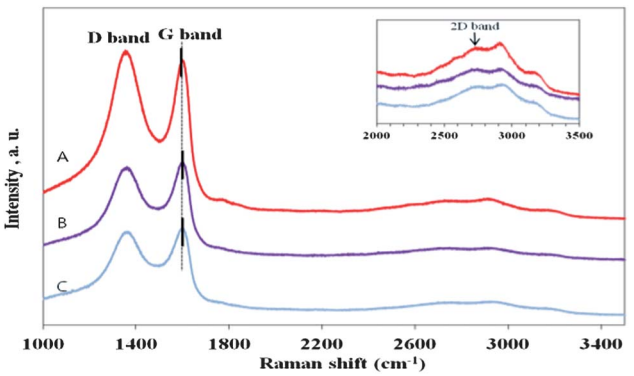

Fig. 7 Raman spectra of GO (A), sample 3 (B) and sample 6 (C), with inset showing the 2D band.

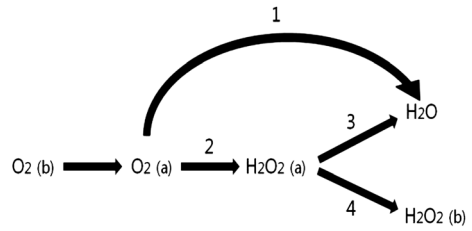

Scheme 1 A model for ORR (a) adsorbed on an electrode surface and (b) in bulk solution.

O_2. The electrocatalytic O_2 reduction activity determined by the RRDE voltammetry method using three samples was investigated in 0.5 M H_2SO_4 solution under O_2-saturated conditions at a rotation speed of 100 rpm. The disk potential employed was from +0.5 V to −0.2 V at 20 mV s^{-1}, and the ring potential was constant at 1.2 V (Fig. 9). The O_2 reduction started at different potentials for different catalysts in the RRDE voltammograms obtained from the GO-*l*-Pt and GO/Pt modified electrodes (Fig. 9A), whereas those obtained from the GO-*l*-Pd and GO/Pd modified electrodes (Fig. 9B) also had distinct O_2 reduction onset potentials. The corresponding synthesized H_2O_2 was re-oxidized at the ring electrodes. The resulting RRDE voltammograms also supported the CV result, in which the longer carbon chain linked GO-*l*-Pt and/or GO-*l*-Pd catalysts showed better activity. Also GO-*l*-Pt and GO-*l*-Pd are better catalysts than GO/Pt and GO/Pd.

To verify the ORR pathway, a Koutecky–Levich plot can be used. The Koutecky–Levich equation[42] was used for the calculation of the *n* value as follows:

$$i_{\lim} = 0.62nFAD^{2/3}C\omega^{1/2}\nu^{-1/6} \quad (1)$$

where $i_{\lim}$ is the limiting current (μA) on the plateau, ω the angular velocity (rad s^{-1}), ν the kinematic viscosity (0.01 cm^2 s^{-1}) and *n* the electron number. The Koutecky–Levich plots for the RRDE voltammograms of GO-*l*-NPs obtained at various angular velocities are shown in Fig. 10. The solid lines were obtained from the plateau current. The dependence of the transferred electrons on the cathodic potential was calculated from eqn (1). According to the *n* value, a four-electron transfer was involved, which revealed H_2O as the main product.

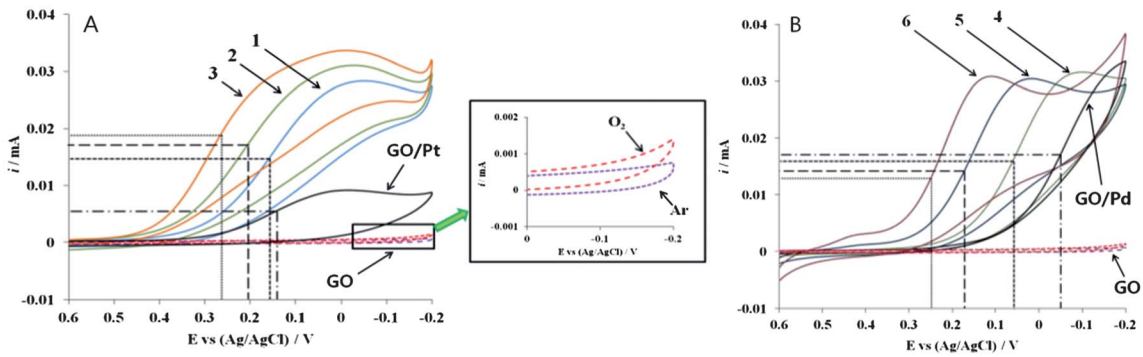

Fig. 8 (A) CVs of GO-*l*-Pt modified GCEs in samples (1), (2), (3), GO and GO/Pt, (B) CVs of GO-*l*-Pd modified GCEs in samples (4), (5), (6), GO and GO/Pd in O_2-saturated 0.5 M H_2SO_4 solution at 100 mV s^{-1}.

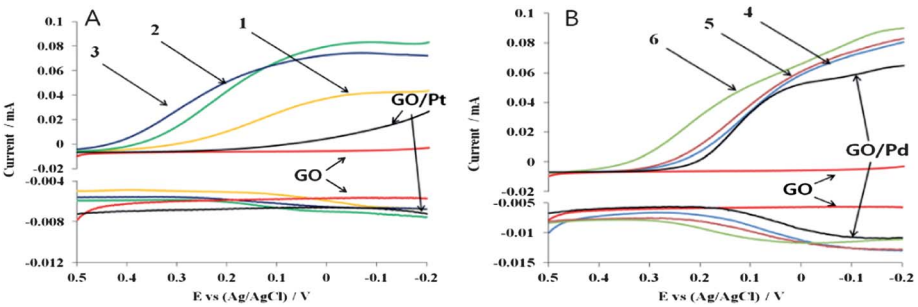

Fig. 9 RRDEs for oxygen reduction on (A) samples (1), (2), (3), GO and GO/Pt, (B) samples (4), (5), (6), GO and GO/Pd. The measurements were carried out in O_2-saturated 0.5 M H_2SO_4 acid solution at a scan rate of 20 mV s^{-1} at 100 rpm rotation. The ring electrode potential was constant at 1.2 V.

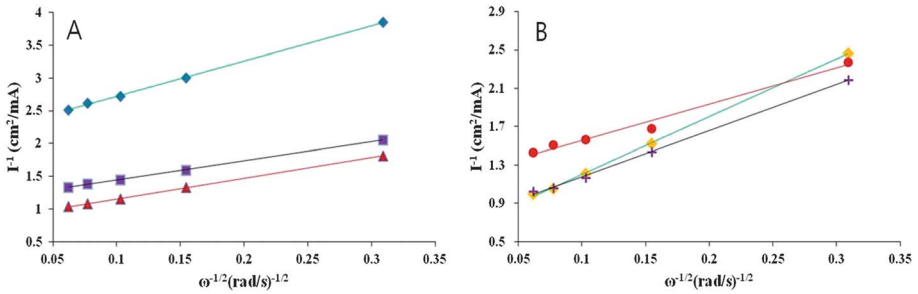

Fig. 10 Koutecky–Levich plots for (A) GO-*l*-Pt: ◆, sample (1); ▲, sample (2); ■, sample (3) and (B) GO-*l*-Pd: ◆, sample (4); ●, sample (5); +, sample (6) at 0.0 V.

Table 2 Comparison of Koutecky–Levich plots for GO–Pt and GO–Pd

Name	*n* Value at −0.1 V	Slope	R^2	Name	*n* Value at −0.1 V	Slope	R^2
Sample 1	2.6	5.37	0.999	Sample 4	3.7	6.01	0.999
Sample 2	4.2	3.27	0.999	Sample 5	3.8	3.78	0.983
Sample 3	3.8	2.92	0.999	Sample 6	4.1	2.82	0.998

Nevertheless, the intercept values do not approach 0 and the plots have a distinct slope. The results indicated that ORR was not controlled solely by diffusion-limited processes.[43] Table 2 summarizes the Koutecky–Levich plots.

Conclusions

The effect of the length of the linker Pt/Pd decoration of GO on the catalytic activity towards ORR was investigated. Six samples were prepared with three different linker molecules, $HS(CH_2)_2SH$, $HS(CH_2)_3SH$ and $HS(CH_2)_4SH$, and two different metal NPs, Pt and Pd. The kinetics of cathodic O_2 reduction were examined for GO–Pt- and GO–Pd-modified GCE catalysts. A combination of CV, RRDE voltammetry and TEM techniques was used to investigate the behavior of the GO-*l*-Pt and GO-*l*-Pd-modified GCE catalysts for ORR in 0.5 M H_2SO_4 aqueous solutions. The study covered a potential range between 0.6 V and −0.2 V (for CV) with attention given to the ORR process. The longer linker samples (3) and (6) exhibited half-potentials of +0.29 V and +0.25 V, respectively. Using the chain to widen the surface area of crumpled GO, metal nanoparticles are attached to the wide area. The atomic% of the long chain containing linker metals was increased and their high catalytic activity was observed. Voltammetry was used to determine the kinetic parameters for O_2 reduction and to detect intermediate H_2O_2 formation. ORR started from a positive potential (0.4 V, RRDE). The Koutecky–Levich equation and plots were used to determine the transferred electrons and to verify that ORR was not diffusion controlled. The CV and RRDE voltammetry results showed that the catalysts with longer chains (samples 3 and 6) had superior catalytic activity towards ORR. The RRDE results confirmed that water was the major product of O_2 reduction by the GO-*l*-NPs-modified GCE *via* four-electron transfer.

Acknowledgements

This research was supported by the science research program through the National Research Foundation of Korea (NRF) funded by the Ministry of Education, Science and Technology (2010–0007864).

Notes and references

1 M. R. Tarasevich, A. Sadkowski and E. Yeager, in *Comprehensive Treatise of Electrochemistry*, ed. B. E. Conway, J. O'M. Bockris, E. Yeager, S. U. M. Khan and R. E. White, Plenum Press, New York, 1983, vol. 7, pp. 301–398.

2 R. R. Adzic, Frontiers in Electrochemistry, in *Electrocatalysis*, ed. J.Lipkowski and P. N. Ross, VCH Publishers, New York, 1998, vol. 5, p. 197.
3 S. Gottesfeld and T. A. Zawodzinski, in *Advances in Electrochemical Science and Engineering*, ed. R. C. Alkire and D. M. Kolb, Wiley-VCH, Weinham, 1997, vol. 5.
4 F. Bidault, D. J. L. Brett, P. H. Middleton and N. P. Brandon, *J. Power Sources*, 2009, **187**, 39–48.
5 J. Guo, A. Hsu, D. Chu and R. Chen, *J. Phys. Chem. C*, 2010, **114**, 4324–4330.
6 H. J. Kim, Y. S. Kim, M. H. Seo, S. M. Choi, J. M. Cho, G. W. Huber and W. B. Kim, *Electrochem. Commun.*, 2010, **12**, 32–35.
7 J. Zhang, Y. Mo, M. B. Vukmirovic, R. Klie, K. Sasaki and R. R. Adzic, *J. Phys. Chem. B*, 2004, **108**, 10955–10964.
8 K. S. Novoselov, A. K. Geim, S. V. Morozov, D. Jiang, Y. Zhang, S. V. Dubonos, I. V. Grigorieva and A. A. Firsov, *Science*, 2004, **306**, 666–669.
9 A. K. Geim and K. S. Novoselov, *Nat. Mater.*, 2007, **6**, 183–191.
10 J. F. Wang, S. L. Yang, D. Y. Guo, P. Yu, D. Li, J. S. Ye and L. Q. Mao, *Electrochem. Commun.*, 2009, **11**, 1892–1895.
11 M. D. Stoller, S. J. Park, Y. W. Zhu, J. H. An and R. S. Ruoff, *Nano Lett.*, 2008, **8**, 3498–3502.
12 Y. Wang, Y. Wan and D. Zhang, *Electrochem. Commun.*, 2010, **12**, 187–190.
13 M. J. McAllister, J. L. Li, D. H. Adamson, H. C. Schniepp, A. A. Abdala, J. Liu, M. Herrera-Alonso, D. L. Milius, R. Car, R. K. Prud'homme and I. A. Aksay, *Chem. Mater.*, 2007, **19**, 4396–4404.
14 J. Y. Kim, K. Park, S. Y. Bae, G. C. Kim, S. Lee and H. C. Choi, *J. Mater. Chem.*, 2011, **21**, 5999–6005.
15 X. Li, X. Wang, L. Zhang, S. Lee and H. Dai, *Science*, 2008, **319**, 1229.
16 D. Li, M. B. Muller, S. Gilje, R. B. Kaner and G. G. Wallace, *Nat. Nanotechnol.*, 2008, **3**, 101–105.
17 Y. Si and E. T. Samulski, *Nano Lett.*, 2008, **8**, 1679–1682.
18 B. Erable, I. Vandecandelaere, M. Faimali, M. L. Delia, L. Etcheverry, P. Vandamme and A. Bergel, *Bioelectrochemistry*, 2010, **78**, 51–56.
19 T. Toda, H. Igarashi and M. J. Watanabe, *Electroanal. Chem.*, 1999, **460**, 258.
20 U. A. Paulus, A. Wokaun, G. G. Scherer, T. J. Schmidt, V. Stamenkovic, N. M. Markovic and P. N. Ross, *Electrochim. Acta*, 2002, **47**, 3787.
21 M. H. Seo, S. M. Choi, H. J. Kim and W. B. Kim, *Electrochem. Commun.*, 2011, **13**, 182–185.
22 K. J. J. Mayrhofer, D. Strmcnik, B. B. Blizanac, V. Stamenkovic, M. Arenz and N. M. Markovic, *Electrochim. Acta*, 2008, **53**, 3181–3188.
23 J. Perez, E. R. Gonzalez and E. A. Ticianelli, *Electrochim. Acta*, 1998, **44**, 1329–1339.
24 M. H. Seo, S. M. Choi, H. J. Kim, J. H. Kim, B. K. Cho and W. B. Kim, *J. Power Sources*, 2008, **179**, 81–86.
25 J. Wu, Y. Wang, D. Zhang and B. Hou, *J. Power Sources*, 2011, **196**, 1141–1144.
26 S. Woo, Y. R. Kim, T. D. Chung, Y. Piao and H. Kim, *Electrochim. Acta*, 2012, **59**, 509–514.
27 S. Y. Yang, K. H. Chang, H. W. Tien, Y. F. Lee, S. M. Li, Y. S. Wang, J. Y. Wang, C. C. M. Ma and C. C. Hu, *J. Mater. Chem.*, 2011, **21**, 2374–2380.
28 C. Xu, X. Wang and J. W. Zhu, *J. Phys. Chem. C*, 2008, **112**(50), 19841–19845.
29 Y. Li, W. Gao, L. Ci, C. Wang and P. M. Ajayan, *Carbon*, 2010, **48**, 1124–1130.
30 C. V. Rao, A. L. M. Reddy, Y. Ishikawa and P. M. Ajayan, *Carbon*, 2011, **49**, 931–936.
31 D. C. Marcano, D. V. Kosynkin, J. M. Berlin, A. Sinitskii, Z. Sun, A. Slesarev, L. B. Alemany, W. Lu and J. M. Tour, *ACS Nano*, 2010, **4**, 4806–4814.
32 J. Maruyama, M. Inaba and Z. Ogumi, *J. Electroanal. Chem.*, 1998, **458**, 175–182.
33 J. M. You, D. Kim and S. Jeon, *Electrochim. Acta*, 2012, **65**, 288–293.
34 L. M. Ioffe, P. Bosch, T. Viveros, H. Sanchez and Y. G. Borodko, *Mater. Chem. Phys.*, 1997, **51**, 269–275.
35 F. Coccia, L. Tonucci, D. Bosco, M. Bressan and N. d'Alessandro, *Green Chem.*, 2012, **14**, 1073–1078.
36 K. Zhang, Q. Yue, G. Chen, Y. Zhai, L. Wang, H. Wang, J. Zhao, J. Liu, J. Jia and H. Li, *J. Phys. Chem. C*, 2011, **115**, 379–389.
37 K. Winkler, K. Noworyta, A. B-Dias, J. W. Sobczak, C. T. Wu, L. C. Chen, W. Kunter and A. L. Balch, *J. Mater. Chem.*, 2003, **13**, 518–525.
38 C. S. Liao, C. T. Liao, C. Y. Tso and H. J. Shy, *Mater. Chem. Phys.*, 2011, **130**, 270–274.
39 W. He, H. Jiang, Y. Zhou, S. Yang, X. Xue, Z. Zou, X. Zhang, D. L. Akins and H. Yang, *Carbon*, 2012, **50**, 265–274.
40 Y. Hu, H. Zhang, P. Wu, H. Zhang, B. Zhou and C. Cai, *Phys. Chem. Chem. Phys.*, 2011, **13**, 4083–4094.
41 A. Damjanovic, M. A. Genshaw and J. O. M. Bockris, *J. Chem. Phys.*, 1966, **45**, 4057.
42 D. T. Sawyer, A. Sobkowiak and J. L. Roberts Jr., *Electrochemistry for Chemists*, John Wiley & Sons, New York, 2nd edn, 1995.
43 R. H. Castellanos, A. L. Ocampo, J. Moreira-Acosta and P. J. Sebastian, *Int. J. Hydrogen Energy*, 2001, **26**, 1301–1306.

